Simulations of Electric Fields within a Thunderstorm

WILLIAM W. HAGER,* JOHN S. NISBET,† JOHN R. KASHA,† AND WEI-CHANG SHANN‡

*Mathematics Department, University of Florida, Gainesville, Florida
†Communications and Space Sciences Laboratory, Department of Electrical Engineering, The Pennsylvania State University, University Park, Pennsylvania
‡Mathematics Department, The Pennsylvania State University, University Park, Pennsylvania

(Manuscript received 12 January 1989, in final form 15 May 1989)

ABSTRACT

Numerical simulations based on a three-dimensional model for the electric fields in a thunderstorm are presented. In some of the simulations, we solve problems with known analytical solutions in order to determine the relevant physical properties that must be incorporated in a thunderstorm model. We then examine the inverse problem: Given measurements for the electric fields in a thunderstorm, what are the associated current generators? Fits based on an analytic formula that neglects conduction currents give approximations to the current generators while simulations based on the thunderstorm model yield refinements to the generators. As a specific illustration, we obtain estimates for current generators associated with a storm observed at the Kennedy Space Center on 11 July 1978. Finally, we explore qualitative properties of our method used to simulate lightning. It is observed that as the charged particles associated with the thunderstorm are spread over a larger and larger volume, the flash rate decreases while the charge transfer associated with each flash increases. Also, it is seen that a series of intracloud flashes can produce a charge imbalance in the cloud that will eventually lead to a cloud-to-ground discharge.

1. Introduction

The electrical environment of an active thunderstorm is very complex. Currents are initiated when a wide spectrum of sizes and habits of charged particles flow in the convective system of the cloud under the influence of gravitational and electric fields. The system is very dynamic because the time constant associated with the change in currents is often shorter than the electrical time constants in and below the cloud; consequently, displacement currents must be considered. Electrical breakdown occurs wherever the critical field strength is exceeded. Charges build up wherever currents flow across conductivity gradients. The conductivity increases rapidly with height so that the current streamlines extend to the ionosphere.

Computer models help us to relate electrical observations to the physical processes in the clouds. Modeling a thunderstorm is not easy since a wide range of temporal and spatial scales are involved; since the currents flow to the ionosphere, the model domain must extend on the order of 100 km vertically and radially to avoid distortion of the densities. Lightning, on the other hand, redistributes charge on very small transverse scales while large velocity gradients of the wind and particles occur over distances on the order of a hundred meters. Thunderstorm cells have a lifetime on the order of an hour while the electrical configuration can be changed by lightning several times a second.

Nisbet (1983) examined by means of simple two-dimensional cylindrically symmetric computer models, the relationships between the configurations and magnitudes of the generative currents associated with thunderstorm cells and the lightning currents. Their relationship to the Maxwell current densities to the ground was examined by Nisbet (1985a) while their relationship to the currents to the ionosphere was examined by Nisbet (1985b). Since height dependent horizontal wind shears are exceedingly important in thunderstorm electrification, a three-dimensional model is needed to simulate real thunderstorm cells.

Browning et al. (1987) have discussed a two-dimensional dynamical electrical model, and Helsdon and Farley (1987a,b) have analyzed a storm up to the first lightning flash using a model in which the microphysics and current systems are coupled. More recently, Helsdon et al. (1988) have extended this model to include a lightning flash. Hager et al. (1989) develop a three-dimensional dynamic electrical model specifically designed to interrelate large-scale current systems caused by charged particle motions inside and outside the cloud and the resulting Maxwell current densities to the ground and to the ionosphere. The model is designed to be flexible enough to simulate complex three-dimensional cloud structure while handling the rapid charge reconfiguration by lightning efficiently. It has

Corresponding author address: Dr. William W. Hager, Department of Mathematics, University of Florida, 201 Walker Hall, Gainesville, FL 32611.

been designed with further development to be completely compatible with present large thermodynamic codes such as those of Chen and Orville (1980), Chiu (1978), Clark (1979), Helsdon (1980), Helsdon and Farley (1987a,b), Illingworth and Latham (1977), Klemp and Wilhelmson (1978), Lin et al. (1980), Miller (1978), Schlesinger (1978), Spangler and Rosenkilde (1979), Tripoli and Cotton [(1980), (1982)], Tzur and Levin (1981), Wagner and Telford (1981), and Ziv and Levin (1974). In the present paper, we do not couple our model with any particular thermodynamic code; instead, we select the locations and magnitudes of the current channels in the cloud that are consistent with the observed Maxwell current densities to the ground.

Hager et al. (1989) give the mathematical background of our model. Nisbet et al. (1987a) present data on rainfall, the radar reflectivities and Doppler velocities, and electric field changes and lightning locations for a thunderstorm in Florida, the Thunderstorm Research International Project (TRIP) storm of 11 July 1978. Nisbet et al. (1987b) analyze the data of Nisbet et al. (1987a) to determine the relations between the observable parameters and the fundamental parameters of the electrical system of the two storm cells. In the present paper, fundamental principles relevant to the numerical simulation of a thunderstorm are developed and the physical characteristics of our model are investigated.

Briefly, our paper is organized as follows: Section 2 reviews the model developed by Hager et al. (1989). Section 3 summarizes some of the basic numerical features that must be incorporated in a numerical model for a thunderstorm. A detailed discussion of the numerical experiments appears in the Appendix. In section 4 we explain how our model can be used to solve the inverse problem: Given the electric fields in a thunderstorm, determine the location and amplitude of the current generators. As a specific illustration, we apply our techniques to the TRIP storm of 11 July 1978. In section 5 we explore qualitative properties of our method used to simulate lightning and we present pictures of lightning flashes generated by the model.

2. The model

By Maxwell's equations, the curl of the magnetic field strength $\mathbf{H}$ is given by

$$\nabla \times \mathbf{H} = \epsilon \frac{\partial \mathbf{E}}{\partial t} + \mathbf{J}_T,$$

where ϵ is the permittivity, $\mathbf{E}$ is the electric field, $\mathbf{J}_T$ the (total) current density associated with charged particles circulating in the domain, and $\epsilon(\partial \mathbf{E}/\partial t)$ the displacement current density. The current density in (1) is given by

$$\mathbf{J}_T = \sum_i q_i n_i \mathbf{v}_i$$

where the summation is over all the classes of charged particles, q_i is the particle charge associated with class i while n_i and $\mathbf{v}_i$ are the number density and particle velocity respectively. The particle velocity is given by the sum

$$\mathbf{v}_i = \mathbf{v}_a + \mathbf{v}_{si} + B_i \mathbf{E}$$

where $\mathbf{v}_a$ is the ambient air velocity, $\mathbf{v}_{si}$ the sedimentation velocity in still air, and B_i the particle mobility.

The quantity $n_i q_i$ evolves according to the equation

$$\frac{\partial (n_i q_i)}{\partial t} = P_i - L_i - \nabla \cdot (n_i q_i \mathbf{v}_i)$$

where P_i is the rate of production and L_i the rate of loss for particles in class i. In principle, the charges, densities, and velocities of each class of particles can be determined provided sufficient information is available concerning the evolution of the wind field and reaction rates. Currently, many important parameters in these equations are uncertain. In the present paper, we utilize current channels in the cloud that are consistent with the observed Maxwell current densities to the ground.

Defining the ambient conductivity σ by

$$\sigma = \sum_i q_i n_i B_i$$

and the convection-sedimentation current density $\mathbf{J}$ by

$$\mathbf{J} = \sum_i q_i n_i (\mathbf{v}_a + \mathbf{v}_{si}),$$

we can write the curl of the magnetic field strength

$$\nabla \times \mathbf{H} = \epsilon \frac{\partial \mathbf{E}}{\partial t} + \sigma \mathbf{E} + \mathbf{J}. \tag{1}$$

In the atmosphere, σ typically depends on the altitude. Moreover, σ depends on the electric field in the following sense: Whenever the electric field reaches some breakdown threshold, σ increases by many orders of magnitude.

To eliminate $\mathbf{H}$ from equation (1), we take the divergence to obtain:

$$\epsilon \nabla \cdot \frac{\partial \mathbf{E}}{\partial t} + \nabla \cdot \sigma \mathbf{E} + \nabla \cdot \mathbf{J} = 0.$$

In this paper, it is assumed that the time derivative of the magnetic field is negligible. Hence, the curl of the electric field is zero, $\nabla \times \mathbf{E} = \mathbf{0}$, and $\mathbf{E}$ is the gradient of a potential ϕ. Substituting $\mathbf{E} = \nabla \phi$ gives

$$\epsilon \frac{\partial \nabla^2 \phi}{\partial t} + \nabla \cdot \sigma \nabla \phi + \nabla \cdot \mathbf{J} = 0 \tag{2}$$

where ∇^2 denotes the Laplacian operator defined by $\nabla^2 = \nabla \cdot \nabla$. Equation (2) must be satisfied in some domain that encloses the thunderstorm. Treating the

earth as a perfect conductor, ϕ vanishes on the surface of the earth. Far from the thundercloud, both ϕ and its gradient tend to zero.

A discrete approximation to (2) is obtained in the following way. First, the domain is partitioned into volume elements. Letting S_i denote the volume element with center P_i, we integrate (2) over S_i and we apply the divergence theorem to get

$$\int_{\partial S_i} \epsilon \frac{\partial \nabla \phi}{\partial t} \cdot \mathbf{dS} + \int_{\partial S_i} \sigma \nabla \phi \cdot \mathbf{dS} + I = 0 \quad (3)$$

where I is the net current leaving S_i and ∂S_i is the boundary of S_i. The time derivative in (3) is discretized using Euler's finite difference approximation and the conduction term is replaced by an averaged quantity to obtain

$$\epsilon \int_{\partial S_i} \frac{\nabla \phi^{n+1} - \nabla \phi^n}{\Delta t} \cdot \mathbf{dS} + \int_{\partial S_i} \sigma^n \times [\mu \nabla \phi^{n+1} + (1 - \mu) \nabla \phi^n] \cdot \mathbf{dS} + I^{n+1/2} = 0 \quad (4)$$

where μ is an arbitrary parameter between 0 and 1, the superscript n denotes the time level t_n, Δt denotes the time step $t_{n+1} - t_n$, and the current term is evaluated at time $\frac{1}{2}(t_{n+1} + t_n)$, which is denoted time level $n + \frac{1}{2}$.

Letting ϕ_i denote the discrete approximation to ϕ at the mesh point P_i, the spatial derivatives in (4) are approximated by centered differences to obtain a matrix-vector relation of the form

$$\mathbf{A}[\Phi^{n+1} - \Phi^n] + \Delta t \mathbf{B}[\mu \Phi^{n+1} + (1 - \mu)\Phi^n] = \Delta t \mathbf{I}^{n+1/2} \quad (5)$$

where Φ denotes the vector with components ϕ_i, $\mathbf{I}^{n+1/2}$ corresponds to the current term of (4), the matrix $\mathbf{A}$ depends on the mesh and the permittivity ϵ, and the matrix $\mathbf{B}$ depends on the mesh and the conductivity σ. If μ is between $\frac{1}{2}$ and 1, then (5) is unconditionally stable while for μ between 0 and $\frac{1}{2}$, (5) is stable if

$$\Delta t \leq \frac{2}{1 - 2\mu} \frac{\epsilon}{\max \sigma}.$$

According to the theory of Hager et al. (1989), the sup-norm error corresponding to the discrete approximation generated by (5) is given by

$$\|\Phi^n - \theta^n\|_\infty \leq C(h^2 + \Delta t^m) \quad (6)$$

for Δt sufficiently small where θ^n denotes the vector whose components are the exact potential evaluated at the mesh points at time level t_n, h denotes the mesh spacing, C can grow like $|\log h|$, and $m = 2$ for the Crank–Nicholson scheme while $m = 1$ for $0 \leq \mu \leq 1$, $\mu \neq \frac{1}{2}$.

With regard to lightning, our main interest at present is in redistributing the charge following a buildup in electric field beyond the breakdown threshold in a manner similar to that effected by lightning. To understand the relation between our method used to handle lightning and what occurs in nature, we examine some similarities and differences. In a cloud-to-ground flash as described by Lin et al. (1980), a stepped leader propagates towards ground when breakdown first occurs. The arc channel is a good conductor with radius smaller than 1 cm. Along its length, it maintains a potential close to that at its point of origin. Consequently, a coronal sheath builds up around the channel. For stepped leaders, the current supplying the charge to the coronal sheath is of the order of 100 A. When the stepped leader gets within a few meters of the ground, electrical breakdown takes place between the leader tip and ground producing an upward propagating discharge of earth potential. A large electric field with a current of order of 10,000 A propagates up the channel between the lower grounded end and upper high voltage region producing ionization. The power in this return stroke makes the channel luminous and causes its rapid expansion, producing thunder. Behind the advancing electric field, the corona sheath collapses and current flows to the ground. The dart leaders that precede subsequent strokes carry less charge and follow the main channels of previous strokes. The dart leaders probably draw small, if any, upward propagating discharges from the earth. According to Plooster (1971), subsequent to each of the current pulses marking the return strokes, there may also exist periods during which low currents (of the order of 100 A) flow for periods of milliseconds. The "mopping up" of the excess charge along the leader channel and perhaps the subsequent transfer of charge within the cloud, appear to occur mainly during periods of persistently low currents.

Although our present model is unable to handle events whose time scale are on the order of the time scale of the leader or return strokes or whose distance scale are on the order of the arc diameter, this does not appear to be of predominant importance for our present purposes. Indeed, these aspects of lightning are secondary to those which control the charge transfer. What does seem to be important are the following:

1) That breakdown takes place wherever the field exceeds the critical value.

2) That charges of the right order of magnitude are transferred between appropriate locations.

3) That after charge has been transferred from a given region, charge continues to be removed from adjacent regions until fields everywhere are below critical values.

4) That the charge deposited along the coronal sheath after the arc is extinguished is realistic.

The method we use to simulate lightning in our model can be described in the following way: Using the discrete potential, an approximation to the electric field along line segments connecting mesh points is computed. For example, an approximation to the

component of the electric field along the line segment connect P_i and P_j evaluated at the midpoint of the line segment is given by

$$\partial_{ij}\phi_i = \frac{\phi_j - \phi_i}{|P_j - P_i|}.$$

Whenever some component of the electric field reaches the breakdown threshold, the conductivity between the corresponding mesh points is taken to infinity. As the conductivity tends to infinity, the potential is adjusted throughout the domain so that in the breakdown region, the potential is constant. This adjustment to the potential often leads to cascades; in the process of equilibrating the potential between two nodes, the electric field between an adjacent pair of nodes reaches the breakdown threshold. As explained by Hager et al. (1989) (also Hager 1989), the adjustment to the potential caused by breakdown in the electric field is given by the formula

$$\Phi^{n+1} = \Phi^n - \mathbf{A}^{-1}\mathbf{W}(\mathbf{W}^T\mathbf{A}^{-1}\mathbf{W})^{-1}\mathbf{W}^T\Phi^n \quad (7)$$

where $\mathbf{W}$ is a matrix with each column completely zero except for 2 entries: a $+1$ entry and a -1 entry corresponding to a pair of adjacent nodes where the electric field has reached the breakdown threshold. Since the time step is essentially zero when breakdown takes place, $t_{n+1} = t_n$.

When modeling the electric potential for a thunderstorm using (2), we modify the boundary conditions to take into account the ionospheric and magnetospheric conductivities that couple the thunderstorm to the "global circuit." In the discrete model, this coupling is accomplished in the following way: Each node on the boundary of the upper surface of the model's domain is connected to the ground by a capacitor in parallel with a resistor and current generator to simulate the global conduction and displacement currents outside the modeled region and the current sources to the ionosphere which maintain the ionospheric potential. In our simulation of the TRIP storm of 11 July 1978, the sum of the resistors and capacitors between the ground and the ionosphere were 145 ohms and 0.046 farads, respectively. The total current between ground and the ionosphere was 1379.3 A.

3. Numerical issues

When simulating the electric fields in a thunderstorm using our model, various numerical issues must be addressed: What is the size of the domain that we need to model? What mesh is needed to achieve some given accuracy and how do approximations to the boundary conditions and variations in the conductivity with altitude affect the computational accuracy? To answer these questions and others, we solved problems with known solutions so that estimates for the error could be determined for various choices of the mesh and the boundary conditions. Our numerical experiments, which are described in the Appendix, tend to support the following conclusions:

1) The model domain must extend on the order of 100 km vertically and radially to achieve between 2 and 3 digit accuracy—even though the thundercloud is only a few kilometers in diameter, the regions of significant current density extend far beyond the cloud boundaries.

2) The mesh in the model must be graded with many mesh points concentrated near the current generators—in regions where charge accumulates and the electric field changes rapidly, a fine mesh is needed.

3) Fewer mesh points are needed in the radial direction than in the vertical direction—the electric field changes more rapidly in the vertical direction than in the horizontal direction.

4) Either Dirichlet or Neumann boundary conditions can be employed along the vertical sides of the domain—the fields approach zero far from the thundercloud and the model seems somewhat insensitive to the far field approximation.

5) The Crank–Nicholson time step is more efficient than the backward difference time step in the period between flashes. During a flash, the voltage increases abruptly in the ionosphere. Due to "stiffness" of equation (3) at high altitudes, the backward difference time step produces a more rapid decay of the high altitude transient than the Crank–Nicholson scheme. On the other hand, the Crank–Nicholson scheme is still very accurate at lower altitudes despite large values for the potential in the ionosphere.

6) The computations should be performed in high precision due to the ill conditioning of the conductivity matrix B caused by the variation in the conductivity with altitude.

4. The Thunderstorm Research International Project (TRIP) storm of 11 July 1978

In this section, we examine the problem of determining the current generators in a thunderstorm that correspond to observed electric fields. Referring to section 2, we see that our model can be used to predict electric fields from given current generators. The problem that we address here is the inverse problem: Given the electric fields, what are the current generators? Of course, if we only measure the electric field at a few points, then there may be many possible current generators that can produce the measured field. Our goal is to determine the simplest configuration of current generators that is consistent with the given data.

During the Thunderstorm Research International Project, the electric field of thunderstorms was measured at points on the ground at the Kennedy Space Center. When trying to determine current generators in the model that correspond to an observed storm, we could try to match the electric fields of the model to the observed electric fields. However, the observed

electric fields exhibit a saw-toothed pattern with a sharp drop at each flash, making it very difficult to match the electric fields. On the other hand, the time derivative of the electric field is nearly constant between flashes. Accordingly, it is much easier to match the derivative of the electric fields for both the model and the experimental data.

It follows from a formula of Wilson [see Eq. (12) in the Appendix] that the derivative of the vertical electric field at the ground due to a current I amperes at altitude H meters is given by

$$\frac{dE_z}{dt} = \frac{10^{10}(1.8HI)}{R^3} \tag{8}$$

where R is the distance in meters from the point on the ground where E is measured to the current source. By linearity, it follows that the derivative of the electric field corresponding to a collection of N current sources can be expressed

$$\frac{dE_z}{dt} = 1.8 \times 10^{10} \sum_{i=1}^{N} \frac{H_i I_i}{R_i^3}. \tag{9}$$

where H_i is the height and I_i is the amplitude of the ith current source, and R_i is the distance to the current source. The case $N = 2$ and $I_1 = -I_2$ corresponds to a dipole.

Our first approximation to the solution of the inverse problem is obtained by selecting parameters in (9) to best match the derivative of the observed electric fields. With $N = 1$, we were not able to obtain a good fit to the derivative of the observed electric fields for the TRIP storm of 11 July 1978. We were much more successful using either a dipole fit or a pair of dipoles ($N = 4$ and $I_1 = I_3 = -I_2 = -I_4$). These fits based on the Wilson formula provide only a rough estimate for the current generators since Wilson's formula neglects crucial factors like conductivity. To further refine our estimates for the current generators, the model is run and linearity is exploited to rescale the generators. For example, after running the model we discover that the Maxwell current densities generated by the model are consistently smaller than the Maxwell current densities obtained from experimental data. If we multiply the amplitude of the current generators in the model by a suitable constant in each 5 min period, then the Maxwell current densities of the model agree much better with the Maxwell current densities obtained from experimental data. These amplification factors, which were around 1.3, can be evaluated by solving a least squares problem: We determined the factor by which to amplify the Maxwell current densities of the model in order to minimize (in the least square sense) the deviation between the model's Maxwell current density and the Maxwell current densities obtained from experimental data. This rescaling process can be performed several times to obtain further refinements to the generators.

Before presenting the current generators that we obtained for the TRIP storm of 11 July 1978, let us summarize some of the factors incorporated in our computer simulation. In our simulation, the ambient conductivity was approximated by the Markson–Bahamas–Reikert profile [see Nisbet (1985b)]. This profile is based on data from Markson up to 5.5 km and data from Reikert for higher altitudes. In the cloud region, the conductivity was 0.05 times the ambient conductivity. The shape of the cloud was determined from tri-Doppler radar measurements. In the TRIP storm, there were two distinct cells, referred to as the northern cell and the southern cell. Based on tri-Doppler radar measurements, the clouds were approximated by fixed (noncircular) cylinders extending from 1.2 to 12 km vertically. In Fig. 1, the heavy solid curves near the shaded region is the boundary of the cloud used in the simulation. The three intensities of shading correspond to different values for the radar reflectivity at 1937 UTC and a 7 km altitude: 10–20 dBZ, 20–30 dBZ, and 30–40 dBZ. All data are presented in a right-handed coordinate system with the y-axis along geographic north, the x-axis along geographic east, the z-axis along the vertical direction, and the origin at the point $x = 16\,764$ m, $y = 449\,580$ m on the Florida grid.

The storm simulation was performed using a pair of cylindrical coordinate systems—one system corresponding to each of the two cells of the storm. The number of θ, r, and z grid points were 12, 14, and 15, respectively. The angle mesh was uniform while the radial and vertical mesh points in kilometers were

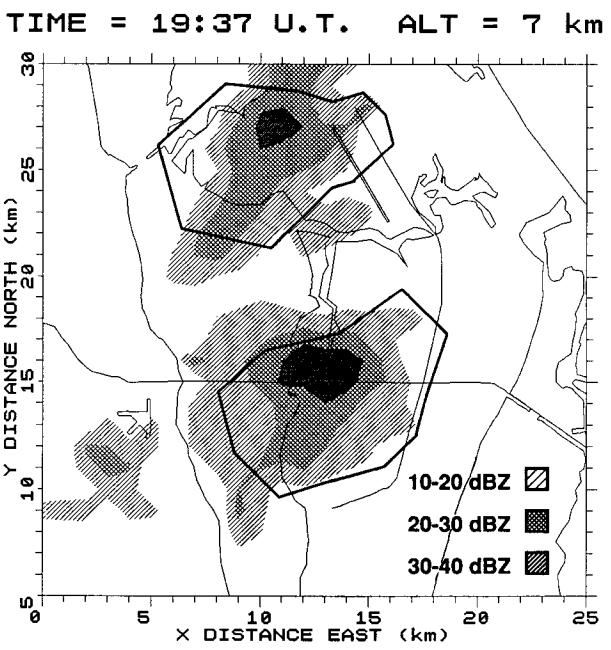

FIG. 1. Radar measurements and the cloud boundary.

r = 1, 1.41, 2, 2.82, 4, 5.64, 8, 11.28, 16, 22.56, 32, 45.12, 64 and z = 0.1, 0.6, 1.2, 2.4, 3.6, 4.8, 6, 7.2, 8.4, 9.6, 10.8, 12, 13.2, 24, 48.

The TRIP storm of 11 July 1978, was partitioned into 5 min intervals, and in each interval, the current generators were treated as fixed (time invariant). For each interval, an average value for dE_z/dt between the flashes was determined at each of the 25 field mills. Using these 25 values for dE_z/dt, the amplitude and the location of the current generators were determined so that the right side of (9), using $N = 2$ or $N = 4$, was as close as possible (in the least squares sense) to the derivative of the observed electric fields. We then ran the model and further refined the current generators by the scaling procedure described previously. The generators that we obtained for the TRIP storm of 11 July 1978, are displayed in Table 1. Column 1 gives the time periods relative to 1900 UTC. For example, the interval 05–10 in column 1 stands for the time period from 1905 to 1910 UTC. The column containing N's and S's indicates whether the current generator is associated with the northern cell or the southern cell. The coordinates of the current generators are relative to the Kennedy Space Center coordinates (see Fig. 1). The tail of a generator is positively charged while the tip of a generator is negatively charged. Figure 2 plots the magnitude of the generator currents associated with the two storm cells as a function of time.

To examine the agreement between the fields associated with the current generators of Table 1 and the observed fields, we compared the Maxwell current density of the model evaluated at the field mills with the Maxwell current densities obtained from the experimental data. At the end of each 5 min interval during the storm, an instant of time was chosen where there were no breakdowns. Since the Maxwell current densities were fairly constant between the flashes, the precise location of this instant is not crucial—it was the end of the time interval unless a flash occurred at the end of the time interval (in which case we positioned the instant before the flash). The Maxwell current density for the storm was estimated at this instant

TABLE 1. Generator currents and locations for northern (N) and southern (S) cells.

Time (1900 UTC)		Tip location (km)			Tail location (km)			Current (A)
		X	Y	Z	X	Y	Z	
05–10	S	14.99	16.57	7.20	12.50	12.24	9.60	.11034
10–15	S	14.99	16.57	7.20	12.50	12.24	9.60	.25501
15–20	S	15.90	15.27	7.20	13.40	10.94	9.60	.33194
	S	16.27	14.90	7.20	13.40	10.94	10.80	.33194
20–25	S	14.40	17.47	7.20	10.44	14.60	9.60	.62132
	S	14.77	17.10	7.20	10.44	14.60	10.80	.62132
25–30	S	15.87	16.60	7.20	13.78	15.4	9.60	1.14320
	N	14.10	24.41	7.20	8.44	23.00	9.60	.04022
	N	13.60	23.87	7.20	9.20	20.17	9.60	.04022
30–35	S	13.90	15.87	7.20	12.17	15.71	9.60	.45990
	S	14.40	15.00	7.20	12.17	15.71	9.60	.45990
	N	13.40	27.10	7.20	8.50	23.27	9.60	.03920
	N	12.90	26.97	7.20	8.50	23.27	9.60	.03920
35–40	S	13.70	15.50	7.20	11.97	15.50	9.60	.33806
	S	14.57	15.00	7.20	11.97	15.50	8.40	.33806
	N	13.30	27.20	7.20	8.40	23.37	9.60	.05318
	N	12.80	27.07	7.20	8.40	23.37	9.60	.05318
40–45	S	13.20	16.07	7.20	14.70	15.20	10.80	.13857
	S	13.57	15.70	7.20	13.41	16.42	10.80	.13857
	N	11.00	23.40	7.20	8.55	23.81	10.80	.13042
	N	10.50	23.27	7.20	8.55	23.81	10.80	.13042
45–50	S	12.50	15.87	7.20	14.45	16.41	10.80	.01398
	S	12.87	15.50	6.00	14.45	16.41	10.80	.01398
	N	12.00	23.70	4.80	10.27	23.70	6.00	.10167
	N	12.00	23.70	4.80	9.55	24.11	7.20	.10167
50–55	S	12.17	18.00	7.20	13.03	18.50	9.60	.04143
	S	12.17	18.00	6.00	12.52	18.20	9.60	.04143
	N	12.60	26.00	6.00	11.60	25.00	7.20	.02882
	N	12.60	26.00	4.80	11.73	26.50	6.00	.02882

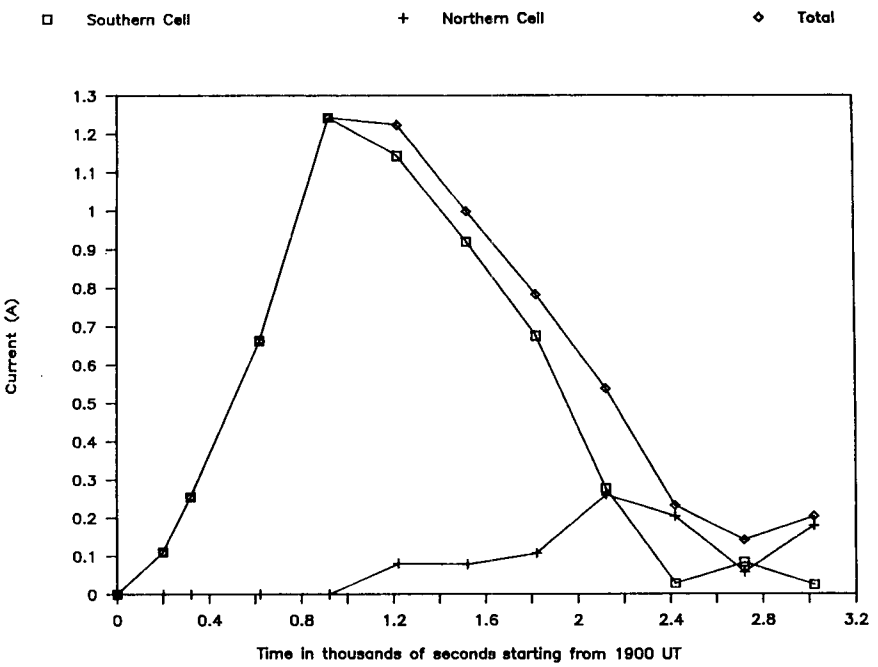

FIG. 2. Generator currents.

in the following way: The rate of change in the electric field in the time period between two flashes was used to approximate the displacement current to the ground. The conduction current density was estimated from the mean electric field assuming a conductivity of 10^{-14} (S/m). Although this value for the conductivity is very uncertain, the conduction current was apparently small enough that exceedingly high conductivities would have been required to greatly affect the estimated total Maxwell current density. In Table 2 we compare the Maxwell current density obtained by the model at the field mill locations to the Maxwell current density obtained from the field mill data. The field mill numbers appear in the first column of Table 2 while the first row of the table indicates the 5 min time period where the Maxwell current densities were measured. Again, time is measured relative to 1900 UTC so that the interval 05–10 is an abbreviation for the time period from 1905 to 1910 UTC. There are two rows corresponding to each field mill. The top row is the Maxwell current density obtained from experimental data while the bottom row is the Maxwell current density generated by the model. Figure 3 gives bar graphs for some of the data in Table 2. It is apparent from Table 2 and Fig. 3 that the model has produced Maxwell current densities in agreement with the actual storm.

To measure the agreement between the model and the experimental data more quantitatively, we computed the relative error associated with the data in Table 2. That is, we summed the absolute difference between the model's Maxwell current density in Table 2 and the Maxwell current density obtained from the field mill data, and we divided by the absolute sum of the Maxwell current densities obtained from the field mill data. The relative error was about 0.3 which indicates that in this simulation, the deviation between the model and the experimental results is around 30%.

5. Lightning

In this section we examine some of the qualitative properties of our method used to simulate lightning. The first set of experiments studies the relationship between flash frequency, charge transfer, and the dimensions of the charged regions in a thundercloud. In our computations, the ambient conductivity is $\sigma(z) = 10^{-14}e^{z/5}$, where the altitude z is measured in kilometers, and the breakdown threshold is 250 000 V m^{-1}. We assume that the current per unit volume at position $\mathbf{r}$ is given by

$$A_P e^{-\omega|\mathbf{r}-\mathbf{s}_P|^2} - A_N e^{-\omega|\mathbf{r}-\mathbf{s}_N|^2}, \qquad (10)$$

where $\mathbf{s}_P$ and $\mathbf{s}_N$ are the centers of the positively charged and negatively charged current generators, respectively. This expression for the current generators is similar to the expression employed in the case study of Browning et al. (1987). The parameters A_P and A_N are chosen so that the total current generated by either the positive or the negative charge centers has magnitude 1 A. As ω increases, the current becomes more concentrated at $\mathbf{s}_P$ and $\mathbf{s}_N$. For example, when ω is 1, about 95% of the current associated with the positive ions is contained in the sphere with center $\mathbf{s}_P$ and radius 2 km. Similarly, with $\omega = 4$, the radius of the sphere con-

TABLE 2. Maxwell current densities (nA m^{-2}): Field mill data (top line) and model (bottom line).

Field mill	Time after 1900 UTC (min)									
	05–10	10–15	15–20	20–25	25–30	30–35	35–40	40–45	45–50	50–55
1	0.004	0.009	0.031	0.055	0.095	0.040	0.041	−0.005	−0.014	−0.004
	0.010	0.026	0.095	0.143	0.088	0.061	0.055	0.023	−0.003	−0.002
2	0.021	0.034	0.034	−0.026	0.032	0.025	0.068	0.043	0.031	0.019
	0.003	0.008	0.015	0.017	0.002	−0.012	0.026	0.042	0.008	0.011
3	0.002	0.004	0.024	0.038	0.073	0.046	0.037	0.000	−0.007	−0.005
	0.005	0.015	0.131	0.104	0.061	0.084	0.074	0.020	0.001	−0.002
4	−0.001	−0.004	0.004	0.009	0.036	0.017	0.022	−0.001	−0.009	−0.006
	0.007	0.019	0.062	0.091	0.053	0.038	0.039	0.006	−0.002	−0.002
5	0.021	0.042	0.041	0.023	0.041	0.022	0.054	0.025	0.019	0.078
	0.008	0.019	0.027	0.130	0.058	0.048	0.104	0.115	0.076	0.076
6	0.012	0.017	0.035	0.057	0.090	0.029	0.071	0.059	−0.003	0.022
	0.014	0.034	0.070	0.149	0.105	0.005	0.045	0.087	0.085	0.040
7	0.045	0.047	0.015	−0.039	0.099	0.090	0.061	0.177	0.143	0.127
	0.010	0.024	0.039	0.076	0.018	−0.056	−0.024	0.164	0.018	0.031
8	0.009	0.011	0.035	0.055	0.059	0.044	0.063	0.030	−0.033	−0.013
	0.011	0.026	0.059	0.127	0.091	0.026	0.039	0.035	0.020	0.007
9	0.007	0.015	0.038	0.061	0.057	0.030	0.042	0.008	−0.011	−0.003
	0.013	0.031	0.070	0.143	0.094	0.026	0.034	0.037	0.014	0.006
10	0.044	0.073	0.133	0.287	0.270	0.082	0.223	0.310	0.295	0.086
	0.019	0.047	0.081	0.335	0.154	0.035	0.076	0.234	0.357	0.104
11	0.050	0.103	0.212	0.490	0.298	0.257	0.185	0.200	0.002	0.029
	0.041	0.100	0.204	0.662	0.309	0.081	0.081	0.195	0.263	0.039
12	0.023	0.054	0.159	0.372	0.246	0.124	0.129	0.072	−0.025	−0.016
	0.031	0.072	0.182	0.344	0.274	0.101	0.088	0.096	0.076	0.012
13	0.008	0.013	0.041	0.068	0.060	0.028	0.039	−0.002	−0.012	−0.005
	0.013	0.032	0.077	0.138	0.090	0.019	0.026	0.032	0.010	−0.001
14	0.028	0.060	0.149	0.285	0.211	0.131	0.121	−0.028	−0.017	−0.001
	0.029	0.067	0.162	0.294	0.245	0.046	0.049	0.049	0.018	0.003
15	0.035	0.057	0.275	0.524	0.376	0.219	0.182	0.040	−0.020	0.005
	0.050	0.107	0.253	0.476	0.503	0.213	0.154	0.133	0.073	0.009
16	0.010	0.017	0.042	0.075	0.085	0.034	0.047	−0.007	−0.022	−0.008
	0.012	0.029	0.079	0.145	0.096	0.053	0.049	0.022	0.002	−0.001
17	0.108	0.231	0.674	1.230	0.835	0.211	0.133	0.068	0.012	0.015
	0.098	0.211	0.588	1.009	1.064	0.578	0.341	0.255	0.088	0.042
18	0.098	0.258	0.605	1.373	1.281	0.974	0.502	0.515	0.204	0.138
	0.111	0.243	0.579	1.390	1.163	0.827	0.472	0.451	0.177	0.118
19	0.046	0.096	0.248	0.477	0.452	0.283	0.218	−0.010	−0.013	0.005
	0.037	0.076	0.246	0.442	0.446	0.243	0.177	0.087	0.027	0.003
20	0.073	0.156	0.470	0.848	0.859	0.548	0.475	0.086	−0.047	−0.043
	0.076	0.166	0.437	0.863	0.861	0.518	0.336	0.156	0.017	0.016
21	0.035	0.078	0.212	0.388	0.430	0.308	0.207	−0.002	−0.033	0.008
	0.041	0.098	0.260	0.471	0.454	0.281	0.203	0.081	0.026	0.004
22	0.060	0.172	0.550	0.968	0.928	1.078	0.708	0.385	0.166	0.052
	0.064	0.151	0.519	0.658	0.862	1.077	0.717	0.313	0.089	0.041
23	0.005	0.020	0.102	0.156	0.230	0.221	0.132	0.062	−0.008	0.026
	0.002	0.010	0.095	0.134	0.133	0.235	0.188	0.058	0.022	0.001
24	−0.004	−0.004	−0.003	−0.001	0.026	0.015	0.013	−0.004	−0.009	−0.008
	0.001	0.005	0.060	0.039	0.019	0.025	0.034	0.005	−0.003	−0.001
25	0.001	0.002	0.025	0.049	0.092	0.094	0.053	0.026	0.003	0.001
	−0.002	−0.002	0.024	0.053	0.020	0.056	0.057	0.017	0.009	0.000

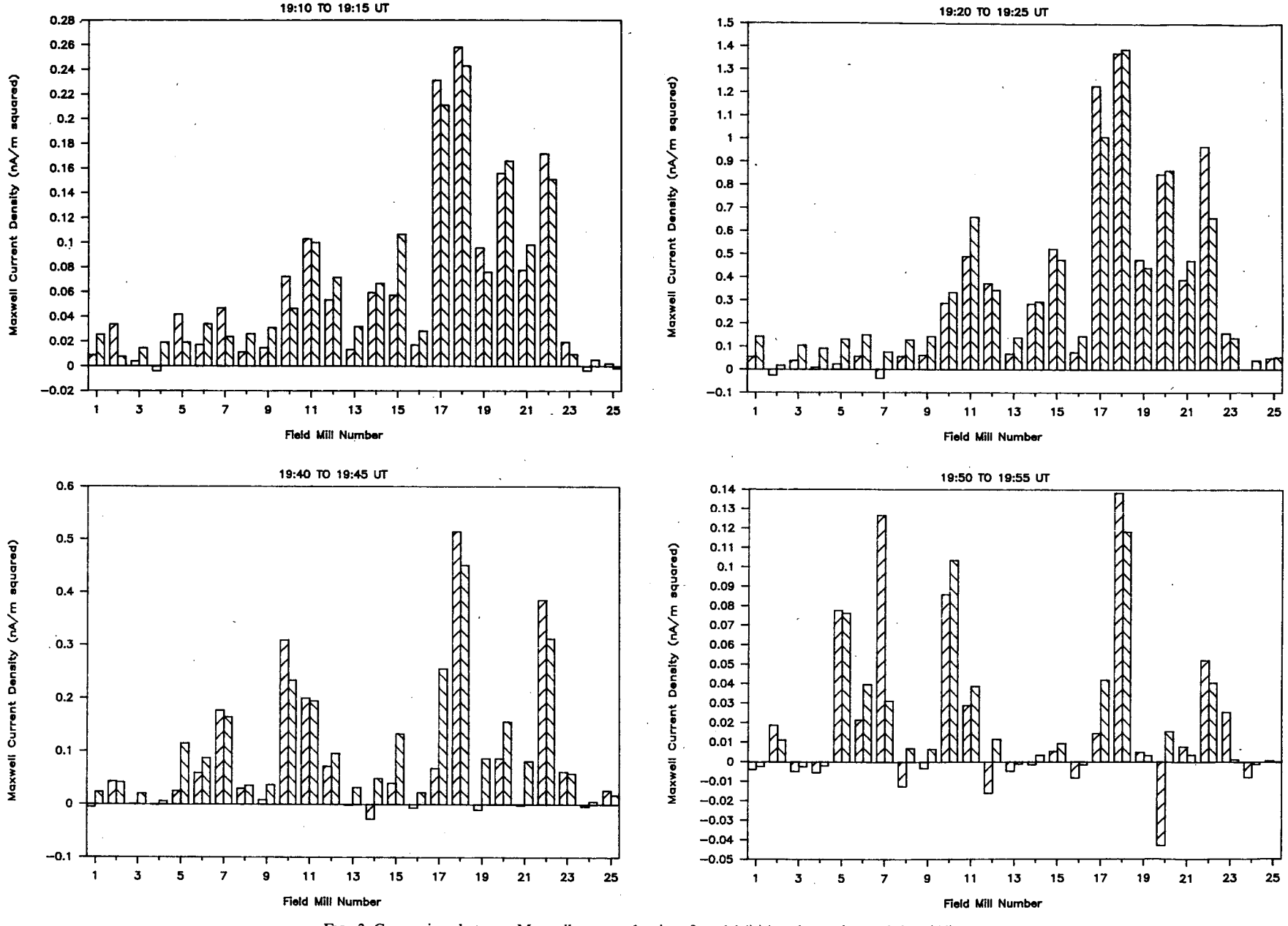

FIG. 3. Comparison between Maxwell current density of model (\\) and experimental data (//).

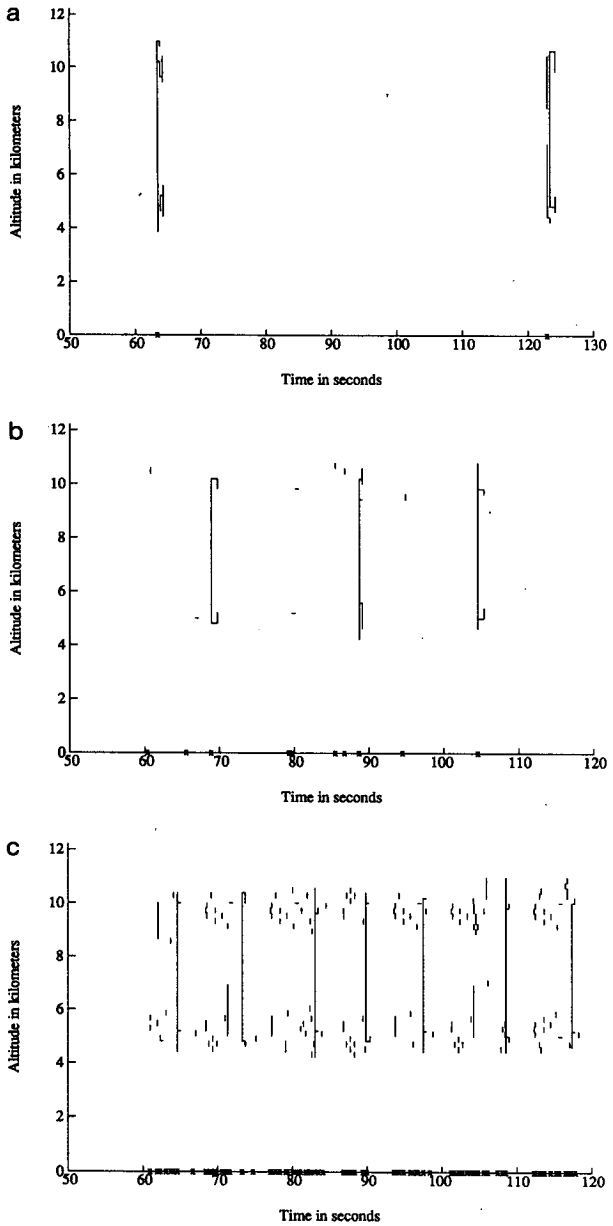

FIG. 4. Breakdown regions corresponding to various current distributions: (a) $\omega = 1$, (b) $\omega = 4$, and (c) $\omega = 16$.

taining 95% of the current is reduced to 1 km. In each experiment, the initial potential is assumed to be zero everywhere. The center of the current generators were positioned on the z-axis, at altitudes 5 km (−) and 10 km (+). The Crank–Nicholson time step was employed, $\Delta t = 1/16$ s, and the mesh was given by (13) and (14) with $m = 96$ and $n = 156$.

The breakdown region corresponding to $\omega = 1$, 4, and 16 and the time period between 60 and 120 seconds appears in Figure 4. The breakdown region is depicted in the following way: Whenever the electric field reaches the breakdown threshold, an "x" is placed at the corresponding time on the horizontal axis. Treating this "x" as the origin for a rectangular $r - z$ coordinate system (the z-axis is vertical and the r-axis points to the right), we draw line segments connecting the nodes corresponding to the breakdown region. For example, we see in Fig. 4a that the electric field reaches the breakdown threshold at about 63 s and the breakdown region extends from just below $r = 0$ and $z = 5$ km to just above $r = 0$ and $z = 10$ km. Also, at $z = 5$ km and at $z = 10$ km, the breakdown region extends several nodes away from the axis $r = 0$.

Observe that when ω is large and the current is concentrated in a small region, there are many tiny breakdowns as well as almost periodic large breakdowns. The charge transfer associated with these tiny breakdowns is almost zero. As ω decreases and the charge is spread over a larger region, the tiny breakdowns disappear and the big breakdowns become less frequent, but more violent in the sense that the total charge transferred by each flash increases. The charge transfer associated with lightning can be determined using the following observation: Integrating the normal component of the electric field around a large cylinder that contains a current generator and applying Gauss's law, we obtain the total charge contained in the cylinder. The total charge increases until the breakdown threshold is achieved. The ensuing flash leads to an abrupt drop in the charge. The magnitude of this drop is the charge transfer associated with the flash of lightning.

Since there are two charge centers for the experiments depicted in Fig. 4, we employed a pair of cylinders, each with radius 5 km and height 7.5 km, centered along the z-axis. The first cylinder extends from $z = 0$ to $z = 7.5$ km while the second cylinder extends from $z = 7.5$ to $z = 15$ km. The charge contained in each of these cylinders is plotted in Fig. 5 for $\omega = 4$ and for time between 60 and 75 s. The total charge associated with the top, positively charged cylinder appears above the horizontal axis while the total charge associated with the bottom, negatively charged cylinder appears below the horizontal axis. The drop in charge at about 69 s is around 18.7 C. Hence, the charge

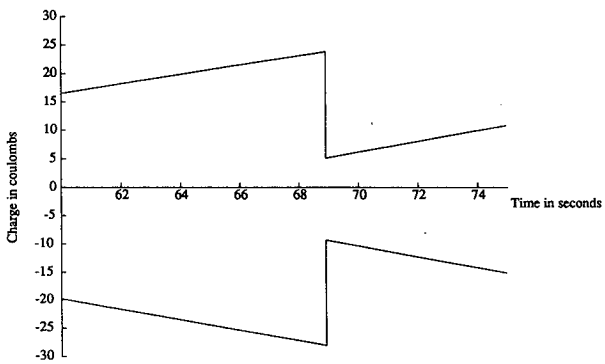

FIG. 5. Positive and negative charge accumulation for $\omega = 4$.

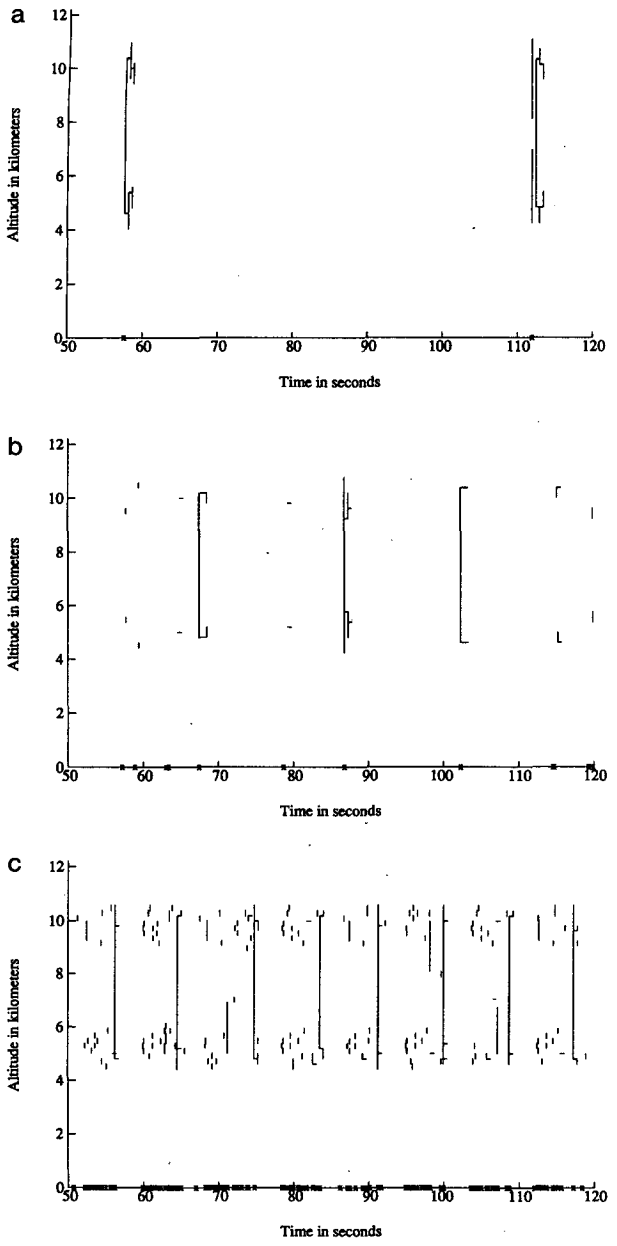

FIG. 6. Breakdown regions corresponding to reduced conductivity in the cloud and various current distributions: (a) $\omega = 1$, (b) $\omega = 4$, and (c) $\omega = 16$.

transfer associated with the lightning flash is about 18.7 C. As the charge becomes more concentrated, the flash frequency increases and the charge transfer decreases. With $\omega = 16$, the charge transfer associated with the 7 flashes of Fig. 4c are 7.6, 9.0, 9.0, 6.2, 7.3, 10.9, and 8.0 C. With $\omega = 1$, the charge transfer associated with the 2 flashes of Fig. 4a is 35.8 and 44.1 C.

Next, we consider the effect of reducing conductivity in the part of the thunderstorm corresponding to the cloud. To simulate a cloud, we multiply the ambient conductivity by the factor 0.05 inside the cylinder with radius 5 km extending from 1.2 km to 12 km in altitude. The three simulations of Fig. 4 were repeated using this new structure for the conductivity. Figure 6 is the analogue of Fig. 4 corresponding to the reduced conductivity in the cloud region. The reduction in conductivity leads to more frequent flashes and larger cloud discharges. For example, in Fig. 4a the first discharge occurs at 63.4 s while the corresponding discharge in Fig. 6a occurs at 57.6 s. The first discharge of Fig. 4a transfers about 35.8 C while the first discharge of Fig. 6a transfers about 37.1 C. If the simulation is continued for 412 s, then for the ambient conductivity profile, there are 7 flashes with an average charge transfer of 42.0 C per flash. When the ambient conductivity is reduced by the factor 0.05 in the cloud region, there are 8 flashes with an average charge transfer of 44.6 C per flash.

Observe that the cloud discharges depicted in Figs. 4 and 6 are cloud-to-cloud discharges. If the simulations are continued for several hundred seconds, the conditions for a cloud to ground flash become more favorable, although a cloud to ground flash is never quite achieved. In Fig. 7 we give the analogue of Fig. 5, the charge accumulation figure, for the first 800 s of the simulation corresponding to $\omega = 1$ and the ambient conductivity. As time progresses, the lower (negatively charged) region accumulates more charge than the upper region. If this charge imbalance becomes large enough, then a cloud-to-ground flash is produced. The reason for this imbalance is that at the higher altitude, the conductivity is larger; hence, charge is conducted away from the upper current generator faster than it is conducted away from the lower current generator. With minor changes in the generator structure, cloud-to-ground lightning becomes possible.

One way to obtain a cloud-to-ground discharge is to move the bottom generator closer to the ground. This occurs naturally in storm cells when the heavier charge carriers fall under gravity or when charged particles are trapped in downdrafts. Another way to achieve a cloud-to-ground discharge involves modifying the charge distribution near the base of the thundercloud. Experimentally [see Uman and Krider (1982)], it is observed that a small region of positive charge often occurs at the base of a thundercloud. This effect could be produced by boundary layer charges at the bottom of the cloud, in which case no additional generator is required,

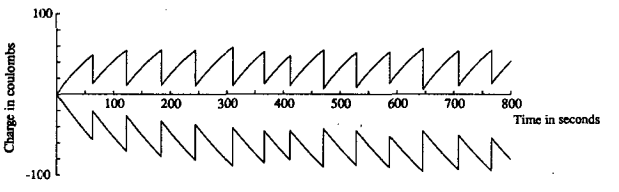

FIG. 7. Positive and negative charge accumulation for $\omega = 1$.

or by an additional current source. To simulate this positive charge at the base of a thundercloud, an extra term was added to the expression (10) for the current per unit volume giving us:

$$A_b e^{-\omega|\mathbf{r}-\mathbf{s}_b|^2} + A_P e^{-\omega|\mathbf{r}-\mathbf{s}_P|^2} - A_N e^{-\omega|\mathbf{r}-\mathbf{s}_N|^2}, \quad (11)$$

where the altitude corresponding to $\mathbf{s}_b$ was 2 km while the amplitude A_b was chosen to make the total current associated with the new generator ¼ A. In Fig. 8 we see that the second flash is a cloud-to-ground flash. The development of this flash in time is shown in Fig. 9. The breakdown begins just beneath the center of the current generator at 5 km. The breakdown proceeds simultaneously above this generator and below the generator, eventually reaching the ground. After reaching the ground, the breakdown continues in the radial direction at the 5 km altitude.

Finally, let us reexamine the scale factors introduced in section 4. Recall that the current estimates obtained from field mill measurements and Wilson's formula were multiplied by a factor around 1.3 when we refined our estimate for the current generators. We feel that much of the discrepancy between the approximation generated by Wilson's formula and the refinement obtained after running the model is due to the fact that

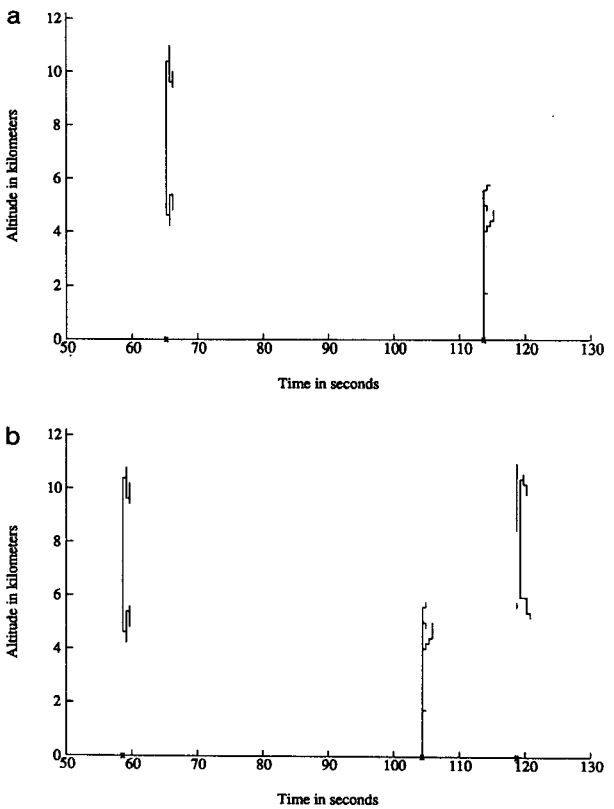

FIG. 8. Breakdown regions corresponding to the currents (11): (a) with ambient conductivity, (b) with conductivity in cloud reduced by the factor 0.05.

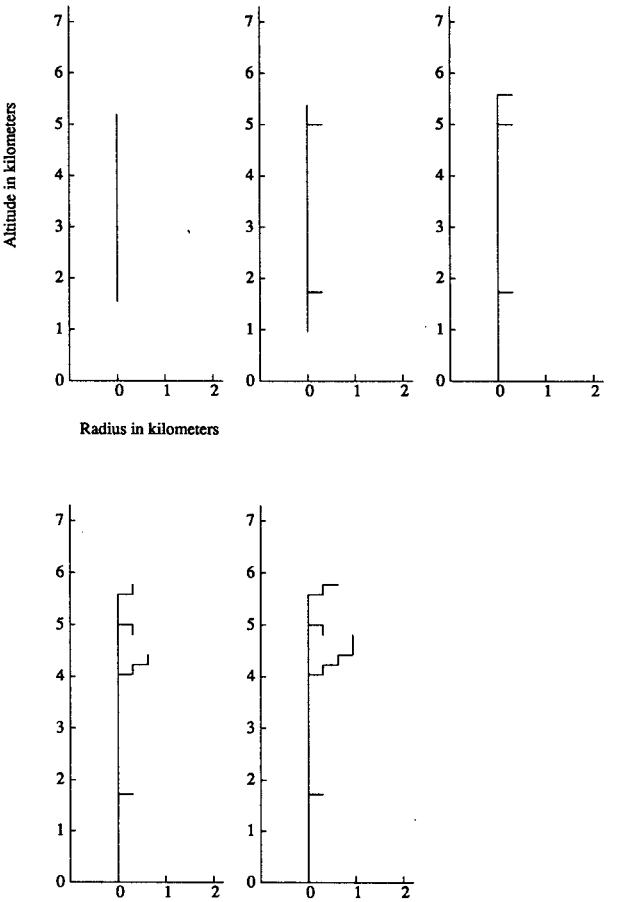

FIG. 9. The cloud-to-ground flash of Fig. 8a.

Wilson's formula neglects conductivity. To investigate the connection between the scale factors of section 4 and conduction effects, let us compute the ratio between the charge transfer associated with lightning and the total generated charge for the simulation reported in Fig. 7. During the first 766 s depicted in Fig. 7, there are 13 flashes transferring about 561 C. On the other hand, the 1 A generators corresponding to this experiment produce 766 C of charge during the first 766 s. Hence, the ratio between the actual charge generated during the simulation and the charge transfer associated with lightning is $766/561 \approx 1.37$, roughly the same as the ratio that was needed to achieve better agreement with the experimental data. As the conductivity of the cloud is reduced relative to the ambient conductivity, the ratio between the generated charge and the charge transfer associated with lightning approaches 1 since less charge leaks from the cloud into the surrounding atmosphere when the conductivity of the cloud is low.

6. Conclusions

In this paper, a three-dimensional numerical model to simulate the electric fields in a thunderstorm was

developed. In our model, we take into account the ionospheric and magnetospheric conductivities that couple the thunderstorm to the "global circuit." This circuit connecting the earth and the ionosphere is absent from other models currently used by meteorologists to analyze cloud electrification. Based on numerical experiments, we found that to simulate accurately the electric fields in a thunderstorm, the domain of the model must extend far beyond the cloud boundaries. The mesh must be graded with many mesh points concentrated near the current generators and with more mesh points in the vertical direction than in the horizontal direction. Either Dirichlet or Neumann boundary conditions can be employed along the vertical sides of the domain. The Crank–Nicholson time step is more efficient than the backward difference time step at lower altitudes, although in the ionosphere, the backward difference scheme is better able to damp out high altitude transients after a flash.

To illustrate the application of the model, we investigated the problem of determining the current generators in a thunderstorm that correspond to observed electric fields. Using initial conditions derived from a least squares fit based on an analytic formula in which conduction currents were neglected, we iterated the location and amplitude of the current generators until agreement was found with current densities at the field mills. As a specific illustration of these techniques, we determined current generators for the TRIP storm of 11 July 1978.

In a second series of simulations, we investigated lightning discharges for symmetric generator configurations. By employing symmetric generator configurations, we were able to compute with high accuracy the evolution of the electric field and the propagation of the breakdown region during a flash. Some of our observations were the following:

1) When the generator current is concentrated in a small region, the model produces both tiny breakdowns which transfer negligible charge and occasional large breakdowns that correspond to lightning. As the generator current is spread over a larger region, these local breakdowns disappear, leaving distinct flashes. As the radius of the sphere containing 95% of the current decreases, the flash frequency increases while the charge transfer associated with each discharge decreases.

2) A series of cloud-to-cloud flashes coupled with variations in conductivity with altitude lead to a charge imbalance with more charge building up near the lower generator. When the charge at the lower generator was large enough, a tiny disturbance could trigger a cloud-to-ground flash. In particular, we saw that a small positive generator placed at the base of the thundercloud could trigger a cloud-to-ground flash.

3) If the conductivity of the cloud is reduced relative to the conductivity of the surrounding atmosphere, both the flash frequency and the charge transfer associated with each flash increase slightly.

APPENDIX

Numerical Experiments

We now describe the numerical experiments that we used to reach the conclusions of section 3. Observe that the coefficient matrix of Φ^{n+1} in (5) is $\mathbf{A} + \mu\Delta t\mathbf{B}$. For small Δt, this coefficient matrix is nearly equal to $\mathbf{A}$. A simple test problem that involves $\mathbf{A}$ by itself is the Wilson impulse problem. Let us consider a current impulse which generates a charge ΔQ coulombs at altitude H meters. By the formula of Wilson (1920), the change in the vertical electric field at a point on the ground R meters from the location of the current impulse is

$$\Delta E = 10^{10}(1.8H\Delta Q)/R^3. \tag{12}$$

In performing our numerical experiments, we took $H = 5000$ m and $\Delta Q = 1$ C, and we used a cylindrical coordinate system—since the electric field changes rapidly with position near the center of a storm and slowly hundreds of kilometers away, a cylindrical coordinate system seems natural for the electric fields. (Later we explain how a superposition of cylindrical coordinate systems can be used when there is more than one charge center.) In a cylindrical coordinate system, the unknowns are the value of the potential at a sequence of nodes positioned on rings around the z-axis. Let z_1 through z_N denote the height of the various rings, let r_1 through r_M denote the ring radii, and let θ_1 through θ_L denote the angles corresponding to nodes in a ring. Hence, the (θ, r, z) coordinates of the nodes have the form (θ_i, r_j, z_k).

For the Wilson impulse problem, the electric potential is symmetric about the z-axis so the discretization in θ is not required. Empirically, we found that the following distribution of mesh points is relatively efficient: If there are m radial grid points $r_1, r_2, \ldots, r_m$ and n vertical grid points $z_1, z_2, \ldots, z_n$, then half the radial and half the vertical grid points are distributed uniformly in the vicinity of the charge center while the remaining grid points are distributed geometrically over the rest of the domain. More precisely, if the altitude of the charge center is H, then the following grid seems to work well:

$$r_j = (j-1)\tau \quad \text{for} \quad 1 \leqslant j \leqslant \frac{m}{2} + 1 \tag{13a}$$

and

$$r_j = 2H + \tau s^{(j-1-m/2)} \quad \text{for} \quad \frac{m}{2} + 1 < j \leqslant m, \tag{13b}$$

where $\tau = 4H/m$ and s is chosen so that $2H + \tau s^{(m-2)/2}$ is the radius of the domain. The grid along the z-axis is chosen in a similar manner:

$$z_k = k\tau \quad \text{for} \quad 1 \leqslant k \leqslant n/2 \quad \text{and}$$

$$z_k = 2H + \tau s^{(k-n/2)} \quad \text{for} \quad \frac{n}{2} < k \leqslant n, \tag{14}$$

where $\tau = 4H/n$ and s is chosen so that $2H + \tau s^{(n/2)}$ is the height of the domain.

To illustrate the importance of grading the mesh, placing a large percentage of the grid points near the charge center, let us consider the error in the numerical solution to the Wilson impulse problem with $H = 5$ km and $\Delta Q = 1$ C using two different meshes: a uniform mesh and the graded mesh given by (13) and (14). In both experiments, the domain is the cylinder given by $0 \leqslant r \leqslant 100$ km and $0 \leqslant z \leqslant 100$ km. Along the bottom boundary $z = 0$ and along the side $r = 100$ km, we impose the Dirichlet boundary condition $\phi = 0$. Along the top boundary $z = 100$ km, we impose the Neumann boundary condition $\partial\phi/\partial z = 0$.

To estimate the error corresponding to various discretizations, we measure the sup-norm relative error in the approximate electric field along the ground. That is, if $\mathbf{E}^h$ denotes the approximate electric field, the error is estimated by the ratio

$$\frac{\underset{\text{(on ground)}}{\text{maximum}}|\mathbf{E} - \mathbf{E}^h|}{\underset{\text{(on ground)}}{\text{maximum}}|\mathbf{E}|}.$$

For the uniform mesh $r_j = (j - 1)(100/79)$ km for $j = 1$ to 80 and $z_k = 1.25k$ km for $k = 1$ to 80, the relative error along the ground is 0.96, and at the specific point $r = z = 0$, the actual electric field is 720 V m^{-1}, while the computed electric field is around 287 V m^{-1}. On the other hand, using the graded mesh (13) and (14) with $m = n = 80$, the relative error is 0.0033 while the computed electric field at $r = z = 0$ is about 717.6 V m^{-1}, which agrees well with the actual electric field 720 V m^{-1}. Hence, it is imperative to grade the mesh to obtain good approximations to the electric field.

Next, let us study how changes in the ratio m/n affect the error. In Table 3 we give the relative error on the ground corresponding to the Wilson impulse problem with $n = 80$ and various choices of m. The last two columns give the time in seconds to factor the matrix **A** and to solve a factored system using the subroutine package SPARSPAK (nested dissection ordering) and a Sun 3/160 microcomputer equipped with a floating point accelerator. As m increases, the computing time increases; however, the error does not improve when m is greater than 50. Hence, there is no advantage in taking m much larger than $n/2$.

TABLE 3. Relative error for Wilson impulse problem with $n = 80$.

m	Error	Factor time	Solve time
20	0.02565	2.34	0.26
30	0.00781	4.26	0.44
40	0.00223	7.30	0.60
50	0.00210	9.82	0.78
60	0.00231	14.00	0.96
70	0.00278	16.94	1.20
80	0.00333	21.22	1.36

TABLE 4. Comparison between solutions computed using Dirichlet and Neumann boundary conditions.

r (km)	Exact electric field (V m^{-1})	Computed field (Dirichlet condition)	Computed field (Neumann condition)
0.00	720.00	721.52	721.62
1.00	678.86	679.31	679.42
2.00	576.30	575.09	575.19
4.00	342.82	341.64	341.75
8.00	107.19	107.06	107.16
15.85	19.60	19.35	19.45
32.95	2.43	2.37	2.48
40.16	1.36	1.32	1.43
49.64	0.72	0.70	0.82
62.10	0.37	0.35	0.48
78.48	0.19	0.16	0.31
100.00	0.09	0.06	0.24

Since both the electric field and the potential approach zero as we move away from a charge cluster, either Dirichlet or Neumann conditions can be imposed on the potential far from the center of charge. Since the electric field approaches zero faster than the potential, one may conjecture that the Neumann boundary condition yields better results. However, there is almost no difference in the relative error corresponding to these two different boundary conditions. For example, let us again consider the cylindrical domain $0 \leqslant r \leqslant 100$ km and $0 \leqslant z \leqslant 100$ km, with the following boundary conditions on the top and bottom of the cylinder: $\phi = 0$ at $z = 0$ and $\partial\phi/\partial z = 0$ at $z = 100$ km. As stated in Table 3, the relative error is 0.00223 with $m = 40$ and $n = 80$ and with the Dirichlet boundary condition $\phi = 0$ at $r = 100$ km (the side of the cylinder). When the boundary condition on the side of the cylinder is changed from the Dirichlet condition to the Neumann condition $\partial\phi/\partial r = 0$, the relative error changes from 0.00223 to 0.00225. Although there is almost no difference between the relative error associated with either Dirichlet or Neumann boundary conditions, the solution computed with Dirichlet boundary conditions tends to be more accurate near the boundary of the domain. For illustration, Table 4 compares the exact electric field to the computed electric field along the plane $z = 0$ with $m = 40$ and $n = 80$.

The accuracy of the computed electric field also depends on the diameter of the domain used in the computation. To investigate the relationship between the domain of the model and the error in the electric field, we consider a cylinder with height 100 km and various radii. Along the bottom and side of the cylinder, Dirichlet boundary conditions are imposed while along the top, a Neumann boundary condition is used. Table

5 gives the relative error on the ground corresponding to various radii for the domain. In performing these experiments, the vertical grid was given by the formula (14) with $n = 80$. In the radial direction, 40 uniform grid points were placed in the region $0 \leq r \leq 10$ km. The remaining grid points were distributed in a geometric fashion using (13b) to fill out the radial domain. As indicated in column 2 of Table 5, the number of radial grid points increases in proportion to the radius of the domain outside 10 km. As the data in Table 5 indicate, there is almost no benefit to extending the radial domain past 100 km when there are 80 mesh points in the vertical direction. In other words, when the domain extends past 100 km, the relative error does not decrease significantly beyond the value 0.0033. Of course, the error depends on both the domain radius and the mesh size. If a finer mesh is used, an increase in the domain radius can decrease the error; and if a coarser mesh is used, decreasing the radius of the domain improves efficiency—the dimension of the discrete problem decreases as we decrease the domain radius while keeping the mesh size fixed.

According to the error estimate (6), the temporal error term is smaller (for tiny time steps) when $\mu = \frac{1}{2}$ (Crank–Nicholson scheme) than for other values of μ. To investigate whether this theoretical superiority in the Crank–Nicholson scheme is actually realized for practical values of Δt, the following experiment was performed: Placing a 1 A current generator at $r = 0$ and $z = 4$ km, the time steps (5) are continued until the first lightning discharge from the cloud (the domain radius and altitude were 100 km, Dirichlet boundary conditions were used along the bottom and side of the cylindrical domain, and Neumann boundary conditions were used along the top). As the time step decreases, the discharge time approaches a limit. Table 6 gives the discharge times for the Crank–Nicholson scheme and various time steps Δt while Table 7 gives the corresponding discharge times for the backward difference time step. Referring to these tables, we see that the limit of the discharge times, as Δt tends to zero, is about 8.935575 s. Subtracting this limit from the computed discharge time gives us the error estimates that appear in the third column of Table 6 and Table 7. From these error estimates, we conclude that the Crank–Nicholson scheme is far superior to the backward difference scheme in this particular experiment—the Crank–Nicholson scheme yields an error of 0.000159 when the time step is $\frac{1}{8}$ s, while to achieve a corresponding error with the backward difference scheme, the time step must be smaller than $\frac{1}{64}$ s.

In a second study of the Crank–Nicholson scheme, we repeated the preceding simulation, but stopped the computer run at $t = 8$ s (just before the first flash). Viewing the potential corresponding to the time step $\frac{1}{128}$ as the "exact" potential, we subtracted it from the potentials corresponding to the smaller time steps to obtain error estimates at all the mesh points. In Table 8 we give the maximum error divided by the maximum potential. Again, when the time step is $\frac{1}{8}$ s, the Crank–Nicholson scheme is an order of magnitude more accurate than the backward difference scheme, and as the time step decreases, the superiority of the Crank–Nicholson scheme becomes more evident.

In both these tests of the Crank–Nicholson scheme, we integrated the equations up to a flash, but not past the flash. During a flash of lightning, the magnitude of the potential increases abruptly in the ionosphere. Since equation (3) becomes stiff at high altitudes, this high altitude transient decays slowly with the Crank–Nicholson. Consequently, after a flash, better approximations to the potential at high altitudes are obtained using the backward difference scheme which is better suited for a stiff equation. To illustrate this property,

TABLE 5. Relative error for Wilson impulse problem and domains of various radii.

Domain radius (km)	m	Error	Factor time	Solve time
25	50	0.00545	10.12	0.78
50	60	0.00369	13.28	1.10
100	80	0.00333	21.22	1.36
200	120	0.00325	34.58	2.10
400	160	0.00323	65.26	3.66

TABLE 6. Discharge time in seconds for the Crank–Nicholson scheme.

Time step (s)	Discharge time	Error
1	8.943574	0.007997
1/2	8.937979	0.002404
1/4	8.936251	0.000676
1/8	8.935734	0.000159
1/16	8.935616	0.000041
1/32	8.935584	0.000009
1/64	8.935577	0.000002
1/128	8.935575	0.000000

TABLE 7. Discharge time in seconds for the backward difference scheme.

Time step (s)	Discharge time	Error
1	8.954765	0.019190
1/2	8.943574	0.007999
1/4	8.939049	0.003474
1/8	8.937134	0.001559
1/16	8.936316	0.000738
1/32	8.935934	0.000359
1/64	8.935752	0.000177
1/128	8.935663	0.000088

TABLE 8. Relative error in the potential at $t = 8$ seconds using the maximum norm.

Time step (s)	Crank-Nicholson error	Backward Euler error
1/2	0.00197	0.00626
1/4	0.00054	0.00265
1/8	0.00013	0.00115
1/16	0.00003	0.00051

TABLE 10. Condition numbers.

	$m = n = 64$		$m = n = 128$	
	Neumann	Dirichlet	Neumann	Dirichlet
A	1.3×10^7	1.3×10^7	1.4×10^8	1.4×10^8
B	1.8×10^{14}	1.7×10^{14}	1.4×10^{15}	1.3×10^{15}

let us consider the simulation corresponding to Fig. 4a; since a lightning flash occurs at about 63 s, we display in Table 9 the value of the potential at 100 km on the z-axis and at 1 s time intervals, starting with 60 s. The time step for the Crank–Nicholson scheme was $1/16$ s while the time step for the backward difference scheme was $1/64$ s.

In Table 9 we see that the potential in the ionosphere jumps to around 4×10^5 after the flash. With the Crank–Nicholson scheme, this high altitude transient decays very slowly while the backward difference scheme drives the potential below 1 after a few seconds. Based on the superior accuracy of the Crank–Nicholson scheme between flashes and the superior stability properties of the backward difference scheme at high altitudes, it follows that a hybrid scheme that uses the Crank–Nicholson scheme between flashes and the backward Euler scheme (with a smaller time step) for a few seconds after each flash (to dampen the high altitude transients) is better than either scheme by itself.

Finally, note that although our numerical experiments produced large values for the potential at high altitudes when the Crank–Nicholson scheme is employed continuously, the values for the potential at lower altitudes seemed to be unaffected by this high altitude stiffness. To illustrate this, Table 9 also displays the value of the potential at 0.2 km on the z-axis. Observe that the values of the potential at 0.2 km associated with the Crank–Nicholson scheme and with the backward difference scheme agree to about 4 significant digits even though the potentials are vastly different at 100 km. In our simulation of the TRIP storm, a storm which lasted nearly 1 h, a (conservative) backward Euler time step was employed. For the lightning simulations of section 5, the Crank–Nicholson time step was employed.

In this Appendix, we have focused on the Wilson impulse test problem. Another fundamental test problem involves computing the vertical Maxwell current density J_M at points on the ground due to a single current generator in the case $\epsilon = 0$ [see Holzer and Saxon (1952) and Nisbet (1985a)]. Numerical experiments based on this problem, which involves only the matrix **B** of (5), yielded similar results. Despite similarities between these two test problems, there is one important difference. Due to variations in σ with altitude, the **B** matrix is more poorly conditioned than the **A** matrix.

Recall [see Hager (1988)] that the condition number of a matrix **M** is given by the product $\|\mathbf{M}\| \, \|\mathbf{M}^{-1}\|$ where $\| \ \|$ denotes a matrix norm. The condition number measures the sensitivity of the solution to a linear system with respect to perturbations in the right side. That is, if the right side **b** of the linear system $\mathbf{Mx} = \mathbf{b}$ is perturbed to $\mathbf{b} + \delta\mathbf{b}$ and if $\mathbf{x} = \delta\mathbf{x}$ denotes the corresponding solution, then we have

$$\frac{\|\delta\mathbf{x}\|}{\|\mathbf{x}\|} \leq \|\mathbf{M}\| \, \|\mathbf{M}^{-1}\| \, \frac{\|\delta\mathbf{b}\|}{\|\mathbf{b}\|}.$$

The condition number of a linear system provides an indication of the accuracy in the computed solution. If the condition number is on the order of 10^c, then potentially on the order of c digits are lost when we solve $\mathbf{Mx} = \mathbf{b}$. Table 10 gives the 1-norm condition

TABLE 9. Computed potential at 100 km and 0.2 km altitude for Fig. 4a.

Time (s)	Crank-Nicholson (100 km)	Backward Euler (100 km)	Crank-Nicholson (0.2 km)	Backward Euler (0.2 km)
60	1.3	1.4	-6.07408×10^6	-6.07401×10^6
61	1.3	1.4	-6.17077×10^6	-6.17070×10^6
62	1.3	1.4	-6.26730×10^6	-6.26722×10^6
63	1.3	1.4	-6.36367×10^6	-6.36359×10^6
64	4.1×10^5	−4.9	-2.68929×10^6	-2.69026×10^6
65	4.0×10^5	−1.5	-2.78485×10^6	-2.78560×10^6
66	3.9×10^5	−0.6	-2.88193×10^6	-2.88259×10^6
67	3.9×10^5	−0.1	-2.97965×10^6	-2.98026×10^6
68	3.8×10^5	0.1	-3.07772×10^6	-3.07829×10^6
69	3.8×10^5	0.3	-3.17600×10^6	-3.17654×10^6

number[1] of the matrices **A** and **B** corresponding to a cylindrical domain with radius 100 km and altitude 100 km and with Dirichlet boundary conditions on the bottom of the cylinder and with Neumann boundary conditions on the top of the cylinder. Either Neumann or Dirichlet boundary conditions were employed on the side and the mesh (13) and (14) was used for the discretization. Observe that the condition number of **B** is much larger than the condition number of **A**. Since double precision corresponds to around 17 digits on many computers, we see that when a linear system $\mathbf{Bx} = \mathbf{b}$ is solved using double precision and $m = n = 128$, nearly every digit can be lost due to rounding errors. Hence, when implementing the scheme (5) with $\mu = \frac{1}{2}$ or $\mu = 1$, it is important to perform the computations in high precision—in single precision, the computed Φ^{n+1} can be completely obscured by numerical errors.

In the numerical experiments described in this section, a cylindrical coordinate system was positioned at the center of charge. However, in a thunderstorm with more than one cell, there will be more than one charge center. To handle these more complex charge distributions, a superposition of cylindrical coordinate systems can be used. Between lightning discharges, the ϕ that satisfies (2) is a linear function of **J** assuming ϕ is initially zero. If **J** is generated by two charge centers, then we can decompose the current density into the form $\mathbf{J}_1 + \mathbf{J}_2$ where the $\mathbf{J}_i$ correspond to the charge centers. We then solve (2) with $\mathbf{J} = \mathbf{J}_1$ or $\mathbf{J} = \mathbf{J}_2$, obtaining solutions ϕ_1 and ϕ_2. Each ϕ_i is computed using a different cylindrical coordinate system positioned at the respective charge center. Finally, $\phi = \phi_1 + \phi_2$.

REFERENCES

Browning, G. L., I. Tzur and R. G. Roble, 1987: A global time-dependent model of thunderstorm electricity. Part I: Mathematical properties of the physical and numerical models. *J. Atmos. Sci.*, **44,** 2166–2177.

Chen, C.-H., and H. D. Orville, 1980: Effects of mesoscale convergence on cloud convection. *J. Appl. Meteor.*, **19,** 256–274.

Chiu, C.-S., 1978: Numerical study of cloud electrification in an axisymmetric, time dependent cloud model. *J. Geophys. Res.*, **83,** 5025–5049.

Clark, T. L., 1979: Numerical simulations with a three-dimensional cloud model: Lateral boundary condition experiments and multicellular severe storm simulations. *J. Atmos. Sci.*, **36,** 2191–2215.

Hager, W. W., 1988: *Applied Numerical Linear Algebra.* Prentice-Hall.

——, 1989: Updating the inverse of a matrix. *SIAM Rev.*, **31,** 221–239.

——, J. S. Nisbet and J. R. Kasha, 1989: The evolution and discharge of electric fields within a thunderstorm. *J. Comput. Phys.*, **82,** 193–217.

Helsdon, J. H., Jr., 1980: Chaff seeding effects in a dynamical-electrical cloud model. *J. Appl. Meteor.*, **19,** 1101–1125.

——, and R. D. Farley, 1987a: A numerical modeling study of a Montana thunderstorm: 1. Model results versus observations involving nonelectric aspects. *J. Geophys. Res.*, **92,** 5645–5659.

——, and ——, 1987b: A numerical modeling study of a Montana thunderstorm: 2. Model results versus observations involving electric aspects. *J. Geophys. Res.*, **92,** 5661–5675.

——, —— and G. Wu, 1988: Lightning parameterization in a storm electrification model. *1988 Proceedings Int. Conf. Atmospheric Electricity,* 849–854.

Holzer, R. E., and D. S. Saxon, 1952: Distribution of electrical conduction currents in the vicinity of thunderstorms. *J. Geophys. Res.*, **57,** 207–216.

Illingworth, A. J., and J. Latham, 1977: Calculations of electric field growth, field structure and charge distributions in thunderstorms. *Quart. J. Roy. Meteor. Soc.*, **103,** 281–295.

Klemp, J. B., and R. B. Wilhelmson, 1978: The simulation of three-dimensional convective storm dynamics. *J. Atmos. Sci.*, **35,** 1070–1096.

Lin, Y. T., M. A. Uman and R. B. Standler, 1980: Lightning return stroke models. *J. Geophys. Res.*, **85,** 1571–1583.

Miller, M. J., 1978: The Hampstead storm: A numerical simulation of a quasi-stationary cumulonimbus system. *Quart. J. Roy. Meteor. Soc.*, **104,** 413–427.

Nisbet, J. S., 1983: A dynamic model of thundercloud electric fields. *J. Atmos. Sci.*, **40,** 2855–2873.

——, 1985a: Thundercloud current determination from measurements at the earth's surface. *J. Geophys. Res.*, **90,** 5840–5856.

——, 1985b: Currents to the ionosphere from thunderstorm generators: A model study. *J. Geophys. Res.*, **90,** 9831–9844.

——, R. A. Barnard, G. S. Forbes, E. P. Krider, R. Lhermitte and C. L. Lennon, 1987: A case study of the TRIP Thunderstorm of July 11, 1978, I. Analysis of the data base. Report number PSU-CSSL-PA-87/12. [Available from Communications and Space Sciences Laboratory, Department of Electrical Engineering, Pennsylvania State University, University Park, Pennsylvania.]

——, J. R. Kasha and G. S. Forbes, 1987: A case study of the TRIP Thunderstorm of July 11, 1978, II. Interrelations among observable parameters controlling electrification. Report number PSU-CSSL-PA-87/13. [Available from Communications and Space Sciences Laboratory, Department of Electrical Engineering, Pennsylvania State University, University Park, Pennsylvania.]

Plooster, M. N., 1971: Numerical model of the return stroke of the lightning discharge. *Phys. Fluids,* **14,** 2124–2133.

Schlesinger, R. E., 1978: A three-dimensional numerical model of an isolated thunderstorm: Part I. Comparative experiments for variable ambient wind shear. *J. Atmos. Sci.*, **35,** 690–713.

Spangler, J. D., and C. E. Rosenkilde, 1979: Infinite cloud model of electrification by the precipitation mechanism in the presence of high rates of ion generation. *J. Geophys. Res.*, **84,** 3184–3190.

Tripoli, G. L., and W. R. Cotton, 1980: A numerical investigation of several factors leading to the observed variable intensity of deep convection over South Florida. *J. Appl. Meteor.*, **19,** 1037–1063.

——, and ——, 1982: Three-dimensional cloud mesoscale model. *J. Rech. Atmos.*, **16,** 185–219.

Tzur, I., and Z. Levin, 1981: Ions and precipitation charging in warm and cold clouds as simulated in one-dimensional time-dependent models. *J. Atmos. Sci.*, **38,** 2444–2461.

Uman, M. A., and E. P. Krider, 1982: A review of natural lightning: Experimental data and modeling. *IEEE Transactions on Electromagn. Compat.*, **24,** 79–104.

Wagner, P. B., and J. W. Telford, 1981: Cloud dynamics and an electric charge separation mechanism in convective clouds. *J. Rech. Atmos.*, **15,** 97–120.

Wilson, C. T. R., III, 1920: Investigations on lightning discharges and on the electric field of thunderstorms. *Philos. Trans. Roy. Soc. London, Ser. A,* **221,** 73–115.

Ziv, A., and Z. Levin, 1974: Thundercloud electrification: Cloud growth and electrical development. *J. Atmos. Sci.*, **31,** 1652–1661.

[1] The 1-norm of a vector is the sum of the absolute value of the components and the 1-norm of a matrix is the maximum of the 1-norms of the columns.